NONINVASIVE ACOUSTOELECTRIC IMAGING OF SPATIOTEMPORALLY VARYING CURRENTS TO DIAGNOSE NEURONAL ELECTRICAL DYSFUNCTION

by

Teodoro Trujillo

A Thesis Submitted to the Faculty of the

DEPARTMENT OF BIOMEDICAL ENGINEERING

In Partial Fulfillment of the Requirements

For the Degree of

MASTER OF SCIENCE

In the Graduate College

THE UNIVERSITY OF ARIZONA

2023

THE UNIVERSITY OF ARIZONA
GRADUATE COLLEGE

As members of the Master's Committee, we certify that we have read the thesis prepared by Teodoro Trujillo, titled NONINVASIVE ACOUSTOELECTRIC IMAGING OF SPATIOTEMPORALLY VARYING CURRENTS TO DIAGNOSE NEURONAL ELECTRICAL DYSFUNCTION and recommend that it be accepted as fulfilling the dissertation requirement for the Master's Degree.

Russell S. Witte
_______________________________ Date: 1/30/23
Russell S. Witte, PhD

_______________________________ Date: 1/30/23
Elizabeth Hutchinson, PhD

Kaveh Laksari
_______________________________ Date: 1/30/23
Kaveh Laksari, PhD

Final approval and acceptance of this thesis is contingent upon the candidate's submission of the final copies of the thesis to the Graduate College.

I hereby certify that I have read this thesis prepared under my direction and recommend that it be accepted as fulfilling the Master's requirement.

Russell S. Witte
_______________________________ Date: 1/30/23
Russell S. Witte, PhD
Master's Thesis Committee Chair
Biomedical Engineering

Acknowledgements

My time at the University of Arizona has taught me that a dream is just a dream, but with discipline and consistency, it becomes a reality. Making a single decision that is not aligned with the path to your success can derail you further than you could imagine. For this reason, I would like to acknowledge the mentors in my life who have provided vision for me when I was blind. I am not impervious, so learning my weaknesses in this time of education has been almost more vital to my success than strengthening my skills.

Father, thank you for giving me what was not given to you. I have always been the one to leap first and ask questions later; but through your wisdom, you've shown me that not all paths deserve my pace. The silver linings of life make it worth living, so milk it. Thank you for the eternal optimism.

Mother, thank you for your mental and physical strength. You epitomize divinity in your commitment to life. Your humor brings love and joy to everyone.

Dr. Witte, without your mentorship, I would be at a loss. Your dedication to questioning the concepts that are some of the most arduous to understand inspires me. The manner of your teaching has taught me confidence when I would normally be fearful.

Alex Alvarez, you are an irreplaceable friend, genuine soul, and graceful leader. Thank you for being an example for me to look up to.

Andrea Anduaga, you always ground my thinking and have helped me in every way possible with my graduate education.

Finally, my sister, thank you for being the friend that tells me exactly what I need to know, when I need to know it; good or bad.

Dedication

I want to dedicate this work to my grandfather, Pete R. Trujillo, who inspired my interest in biomedical engineering with his work in microcellular biology. His inspiration carried me through the graduate process and set precedent for my achievement. I would also like to dedicate this work to my parents for their sacrifice in support of my venture into biomedical engineering. As the son of an architect, success pivots upon, not only on the *function* but the *form* of innovation, tantamount, engineering should account for efficacy and grace. I will exhibit this ethic in my future endeavors as a designer and developer. A mound of failures makes scientific achievement; success is to end standing tall on that mound.

"But we cannot simply sit and stare at our wounds forever."

– Haruki Murakami

…make sure to deeply breathe the beauty of this gift called life.

Table of Contents

Abstract 13

Chapter 1: The Story Behind Neuronal and Cardiac Electrical Dysfunction 15

Background 15

1. *Epilepsy and Parkinson's Disease 15*
2. *Cardiac Arrhythmia 18*
3. *Acoustoelectric (AE) Imaging 19*

Mapping Epilepsy & Atrial Fibrillation with Acoustoelectric Effect 20

Signal and Imaging Processing 21

Medical Need 26

Thesis Aims 27

Chapter 2 – Protocol, Results and Discussion of Spatiotemporal Varying Current tABI Imaging in Human Head DBS Model 30

Methods 30

A. *4D visualization of current travel in human head model 30*

B. *AE Signal Processing 32*

C. *BrainSight and Armature US Targeting System 34*

Results 40

Discussion..45

Chapter 3: Conclusions with Epilepsy Study and Future Work Toward Applicable Cardiac Model............................49

Conclusion..49

Future Work: Cardiac Ex-Vivo Model 53

References **...** 57

Appendix **...** 61

List of Publications...61

List of Figures

Figure 1: Change in electric resistivity is modulated by the introduction of changing US pressure wave which results in a HF detectable voltage (V_{AE}) [3]. Electric resistivity ($\Delta\rho$) is directly related to a tissue's interaction constant and the modulation of acoustic pressure (ΔP) from the US Transducer. --23

Figure 2: The "physiologic"/stimulus waveform consisted of 100-400Hz sinusoids with current magnitude 1mA-30mA enveloped within the shown square waveform. The example AE signals in blue indicate that a signal is created at the depth of current source (red bracket) when the stimulation is on but not when its off. The event trigger (light blue) indicates the start of each scan sequence and controls the feedback loop for stimulation and recording cycle. Many US pulses are sent (black) to increase the AE interaction effect and multiple the sampling effect [25]. --24

Figure 3: Infinity Deep Brain Stimulator (8-channel Infinity 6172ANS, Abbott Inc) shown with two dipoles (S1/S2). Red site is positive, and blue is negative stimulus. Sites have 2mm center to center separation. --31

Figure 4: AdTech Depth Electrode (12-site, SD12R-SP05X-000) with four dipoles shown. Site separation is 5mm center to center, spanning 35mm range. --31

Figure 5: AE signal induced and recorded on gold cup electrode. [A] Diagram shows saline bath with two stimulating electrodes without any current. The ultrasound beam is focused on the positive (+) stimulating electrode. The gold cup picks up any voltage within the bath as is shown in [B]. When Current is injected into the bath[C] the gold cup electrode senses the AE

voltage[D] induced by the interaction of the ultrasound beam and the current gradient within the beam focus [24].--33

Figure 6: User interface for imported Magnetic Resonance (MR) image of head phantom to assist with US targeting of stimulated area (A). Photo of US transducer coupled to head model phantom with agarose gel inside stimulated with DE (B). ---36

Figure 7: MR Image with top-level experimental hardware organization. 4-site stimuli shown with coupled 0.6MHz US transducer. Three HF recording electrodes shown to help with BrainSight MR image overlay geometry with recorded. Recording and filtering Data Acquisition (DAQ) system used to capture three signal inputs for post processing and display purposes.----37

Figure 8: Above is a comprehensive hardware diagram explaining the pathway of the stimulation and recording models. The DBS is shown with 4-dipole connections to the head phantom. The H235 0.6MHz 2D US array is affixed transcranially to the skull with US saline gel. HF recording gold cup electrodes (HF-R_1, HF-R_2) trace from the skull surface to the Preamp board (prototypical filter made in-house) into two channels where HF and LF signals are split. LF current from a diff-amp (measured across 1Ω resistor not shown) is input into another filter board and all signals are taken into National Instruments DAQ and displayed for software processing. Verasonics hardware (UTA 260-S) facilitates US power and trigger regulation feedback loop. BrainSight hardware not shown.--39

Figure 9: (A) 1st Stimulation scenario with vertically positioned DBS: EEG-like waveform with variable frequency profile stimulated with two dipoles on Infinity DBS. (B) The time separation between site stimulation is shown by with dashed-green boxes for each separate stimulated

dipole. (C) Platinum site separation of 2mm (center to center) was visualized with Δd = 1.64mm. --41

Figure 10: 2nd Stimulation scenario using the AdTech 12-site Depth Electrode placed anterior-posterior ~30mm deep from the skull surface. (A) Imported MR images (UTE sequence for enhancing skull contrast) presented here. (B) An exploded view of the detected AE voltages to visualize a transverse horizontal line at 30 mm below the skull surface over stimulation time in msec is shown. The AE polarized image shows the 4 separate locations of stimulation (S1-S4) at varying times each separated center-to-center ~5mm. (C) The LF waveform shows four equivalent three-peak sinusoids corresponding to the four dipoles stimulated on the depth electrode. --42

Figure 11: (A) Low frequency (Orange)/High Frequency (Blue) recorded signal amplitude pk-pk (mA) over time. (B) Signal sensitivity (AE voltage vs. Low Frequency mA) of detected signal versus actual injected signal is extracted. A slope of 1.54 µV/mA is calculated.-------------------44

Figure 12: Because a cinematic cannot be inserted into this document, here is a frame-by-frame process with the red dotted line on the (A) A-line EEG surface trace for time reference. (B) Below the EEG traces the corresponding AE images are mapped with baseband, and the location of the central peak magnitude changed as time continues. This change is relative to the travel of current from S1-S4 dipole locations. The A-line EEG detection above these maps proves this deep brain signal (~30mm) cannot be rectified in the same manner, resolution, accuracy that tABI noninvasive spatiotemporal mapping offers. --46

Figure 13: (A) Frame of cinematic overlay displaying result of tABI image travelling along the implanted DE. Underlay is sagittal view of MR image taken of skull phantom. (B) Zoomed view

of same DE with tABI signal overlayed on MR image from BrainSight. UTE MR sequence used in these figures. ---47

Figure 1414: Plotted above is relative location map of the tracked signals on sites S1-S4 of the AdTech Depth Electrode. The arrows indicate the vector path of travel with their relative velocities. ---50

Figure 15: Sample of in-vivo acute swine studies using bicuculine injection to induce ictal pulses and measure the resultant neuronal reaction. These seizures are global and can help us to continue in development of the swine model and lead into more chronic studies of LF waveform mapping to better understand and diagnose epilepsy in the human model.--------------------------52

Figure 16: Action Potentials and how they anatomically vary; in summation the result is a QRST wave. To better emulate the spatiotemporal travelling of the cardiac current a model was created using the Infinity DBS with 8 sites. --54

Figure 17: Above is the first design for a cardiac electrical model with an embedded DBS Infinity electrode. This design was never made and has potential to be a future step. The different sites correspond to Figure 16 and the respective QRST components. The design that was implemented was a simpler version of this model. This model had an electrically insolated controlled current path that emulated the geometry of the cardiac muscle.--------------------------55

Figure 18: Above is the experimental setup for the first iteration of the cardiac travelling current model. (A) The US Transducer (H235 0.6MHz) is seen affixed to the side of the model with the Infinity DBS in parallel with the long axis (y-axis) of the 2D probe. (B) The stimulation profile included 3-monopoles (S1-S3) with “sinks” in far field (middle green dots). Sites 1, 2A, and 3A

were used on the DBS electrode (bottom middle). (C) The ballistic humimic insulative gel mold was made with a 3D printed form. --- 56

List of Equations

Equation 1 20

Equation 2 21

Equation 3 23

Equation 4 24

Equation 5 25

Equation 6 25

Equation 7 25

Equation 8 26

Abstract

Transcranial Acoustoelectric Brain Imaging (tABI) offers what Scalp Electroencephalography (EEG) alone fails to offer in the complete characterization of epilepsy. Invasive Depth Electrode (DE) EEG techniques may achieve localized detection of neuronal function and noninvasive scalp EEG sacrifices accuracy of signal detection for safety. The goal of this work was defined through noninvasively visualizing travelling current densities of the brain at varying locations and times, determining signal detection limits and calculating conduction velocities of travelling deep neuronal waves. I proposed a method to detect signal profiles that changed over a period of 50 ms and 35mm distance. Neural currents were simulated ex-vivo in a human head model using a 12-site Spencer/AdTech Depth Electrode (DE) and Infinity Deep Brain Stimulator (DBS) with varying current geometries (dipole, monopole). Slow $\leq$ 200 Hz and varying magnitude signals were used to emulate neuronal signals in an agarose/saline gel brain phantom inside a real human skull. TABI movies were produced using a 0.6 MHz center frequency, 2D Ultrasound (US) array. These movies provide demonstrable evidence of effective correction for transcranial US imaging of specific current locations with millimeter (mm) and millisecond (ms) accuracy, more specifically, track these signals as they travel spatially and temporally regardless of their direction of travel. Conduction velocities were found through tracking centroid peak magnitude coordinates (x,y,z) over time to map more effectively specific (1.5mm and 4.5mm site separation on Infinity and AdTech electrodes, respectively) spanning wide field of view (35mm) at sub-cranial depth of ~30mm. Current detection limits were nominally found to be $\leq$300µA. Site to site conduction velocities were

determined to be 4.71 m/s and 3.9 m/s on the *AdTech* and *Infinity* electrodes, respectively. TABI offers a safe, noninvasive, accurate and less expensive route to better track epileptic (ictal) signals, neural degenerative disease, and cardiac fibrillation in the human brain and heart model. In the final chapter of this work, a prototypical cardiac arrhythmia ex-vivo model is described. Baseline tests were made and there remains room for improvement with design ideas listed for better emulation of the heart electrical dysfunction included.

Chapter 1: The Story Behind Neuronal and Cardiac Electrical Dysfunction

Background

The human body without a reliable central and peripheral nervous system is like vehicle without an engine; useful for nothing more than aesthetic. Serving as the communication network, anatomical map for healing and essence of what we define as *living*, the heart and the brain must function reliably to sustain our longevity. The electrical maps of these organs have been the basis of study in medicine and religion since we asked the question: *Where did we come from?* Although there exists many chemical, biological, mechanical, and statistical models to define the human body, electromagnetism transcends all these models. Disorders involving electrical dysfunction can be difficult to diagnose and understand. Imaging has helped us to understand these disorders. Deep tissue electrical mapping has evolved to help in this field but still requires much work to have accurate and streamlined procedure for the treatment of disorders involving the malfunction of the heart and mind. In this work, the focus will be to better understand the complex problematic electrical currents characteristic of epilepsy and cardiac fibrillation; two of the most detrimental nervous system related disorders.

1. Epilepsy and Parkinson's Disease

Epilepsy is characterized by recurrent seizures of partial or generalized involuntary control of peripheral innervation due to abnormal and excessive electrical discharge (ictal) in the central nervous system and in the peripheral nervous pathways. Parkinson's disease is characterized by degradation of the midbrain and dopamine deficiency which result in peripheral muscle tremor. Epilepsy plagues around 50 million people worldwide, and 70 percent of those are believed to be able to live seizure-free lifestyles if correctly diagnosed and treated. 75 percent of epileptic patients live in low-income environments [1]. Ictal activity is variable and can result in petit mal or grand mal seizures which have tonic (muscle stiffness), atonic (muscle relaxation), myoclonic (short spasm) or clonic (periods of spasm) in parts of the body [1]. Within the population of individuals with epilepsy, approximately one in six of these individuals are non-responsive to anti-epileptic drugs and can potentially be treated by neurosurgical treatment [12].

This neurosurgical intervention usually involves ictal correction with a DBS or entire resection of the part of the Central Nervous System (CNS) that is believed to be activating ictal activity. Prior to resection, invasive electrical brain mapping is usually required to estimate the origin of seizure foci and functional brain regions critical to survival (e.g., speech and motor). This method is labor intensive and often inaccurate, especially for deep brain signal detection. Epilepsy along with many other brain disorders, would directly benefit from an innovative noninvasive technique capable of real-time, high resolution electrical imaging of neuronal circuits deep in the human brain.

To better characterize these ictal discharges in the central nervous system many techniques have been developed with varying success. Inherent tradeoffs with electrical brain mapping include:

- Invasiveness vs. Resolution vs. Field-of-view
- Blurring of bioelectric fields through tissue

- Massively under-determined inverse problem

Scalp electroencephalography (EEG) is unable to accurately resolve current densities on the mm scale due to blurring of the electric field as it passes through the brain and skull, leading to an ill-defined and underdetermined inverse problem using surface signals. Invasive EEG (iEEG) has much better capacity for localized and specific neuronal current detection with limited field of view. Another drawback of iEEG is the risk of surgical complication when a Depth Electrode (DE) or Deep Brain Stimulator (DBS) are inserted into the cranium. Magnetoencephalography (MEG) is another option for monitoring deep brain magnetic signals at the centimeter scale; however, the cost is prohibitive and works best when combined with other scalp EEG. To best achieve deep brain signal detection and tracking for treatment of epilepsy, tABI offers a safe and accurate way to noninvasively resolve travelling current densities of the brain at varying locations and times, determine signal detection limits and calculate conduction velocities of travelling deep neuronal waves at the mm and ms resolutions, improving upon EEG.

Epilepsy is a neurological disorder affecting over 50 in 100,000 people every year[1]. The physiological characterization of epilepsy is marked by atypical aberrant activity of neurons and neural groups. Within the population of individuals with epilepsy, approximately one in six of these individuals are non-responsive to anti-epileptic drugs and can potentially be treated by neurosurgical treatment [1]. Presurgical assessment of the treatability of epilepsy through surgical intervention relies on mapping of neural activity and physical structure to characterize the localization of the seizure [1][2][3]. Source Localization is a method of imaging used to recreate spatial and temporal distributions of current activity within the brain with the potential to offer higher spatial resolution improving epilepsy foci identification [4][5]. Mapping by current density imaging methodologies are varied including electroencephalogram (EEG) [4], magnetoencephalography (MEG) [6], micro-electrocorticography (EcoG) [6][5], magnetic resonance imaging (MRI) [7], and ultrasound [8] based methods. EEG and MEG methods suffer from poor reconstruction resolution due to uncertainties in conductivity distributions, while EcoG methods are invasive [7][9][10].

2. Cardiac Arrhythmia

Atrial Fibrillation (AF) is the most common form of abnormal heart rhythm (cardiac arrhythmia). Atrial Fibrillation affects 9% of the US population (2% younger than age 65), contributes to 750,000 hospitalizations and 130,000 deaths per year [19]. This symptom usually occurs when the electrical signals in the atria disorganize and cause a flutter (fibrillation) of the heart muscle in a fashion that prohibits healthy volumetric flow of blood through the heart pump. This dissonance in electrical signal easily results in more complications including embolic stroke, heart failure, and increased mortality [20]. Electrocardiogram (ECG) provides peerless information regarding the consistency of the normal QRST complex from a surface low frequency detection for diagnosis and eventual prognosis for AF. Unfortunately, this surface detection method has its weaknesses. Although ECG can help to illuminate irregular P-wave and QRST complexes it does not possess the diagnostic accuracy for rotor mapping of AF phase information, complex fractionated ECG and disease progression. US pulse echo imaging alone is unable to image electrical pathways, hence, the method of Transthoracic Acoustoelectric Cardiac Imaging (tACI) offers great ability to noninvasively map these spatiotemporally varying electrical currents on an accurate, millisecond and millimeter level that has potential to surpass the capabilities of ECG with the goal of bettering diagnosis and treatment of AF.

Intracardiac catheter radiofrequency (RF) ablation method for treating AF when pharmacological agents fail has proven to be effective. RF ablation has successfully treated many types of stable arrhythmias [19,20]. Despite this fruition, downsides to this invasive treatment still exist. The stressful length of these procedures, invasiveness, and multiple ablations can lead to thermal injury, imbalance of sympathetic and parasympathetic cardiac tone that can all lead to auxiliary cardiac chronic issues [21]. With the Depth Electrode (DE) cardiac model, better characterization of this RF ablation method remains one of the goals to make safer these types of invasive treatments.

3. Acoustoelectric (AE) Imaging

Current source density mapping offers a great benefit to the diagnosis and treatment pathways for epilepsy and atrial fibrillation. The AE method is a novel technique that relies on a high frequency (HF) target signal rather than traditional EEG and ECG low frequency (LF) detection methods. Because this model has not been clinically developed there are many challenges. Some of the major challenges is increasing the field of view, developing a realistic model for testing without relying on live animal models and filtering of a relatively noisy high frequency band (100kHz – 10MHz) to preserve a small AE voltage. In this work I address development of an effective ex-vivo model that directly emulates a clinical epileptic deep brain stimulation/depth electrode treatment monitoring model. In addition, this work shows how AE signal can be collected in a wide field of view (35mm span) at very deep tissue depths (30mm) over time. Signal to noise ratio (SNR) continues to be a variable dependent on test location and ambient noise sources. To address this, an active electrode model is in development and remains a next step. The potential impact of this work can robustly increase the efficacy, reduced treatment time, reduction of invasive treatment and unequivocal accuracy of deep tissue current source mapping for electrical disorder diagnosis.

Mapping Epilepsy & Atrial Fibrillation with Acoustoelectric Effect

Epilepsy is characterized by recurrent seizures of partial or generalized involuntary control of peripheral innervation due to abnormal and excessive electrical discharge (ictal) in the central nervous system. AF is characterized by similar asynchronous electrical pathways to that in the epileptic mechanism; theoretically, benefitting from similar acoustoelectric imaging diagnostics. This physiological signal can be modulated without altering its intrinsic quality. Through an acoustically transmissible medium a phenomenon is seen that dictates a proportionality between variable ultrasound pressure (ΔP) and results in a change of electrical resistivity ($\Delta\rho$):

$$\Delta\rho = K\rho_0\Delta P$$

Equation 1

Where ρ_o represents initial resistivity, K is the interaction constant 0.034 ± 0.003%/MPa in 0.9% NaCl solution and 0.041 ± 0.012%/MPa in rabbit heart tissue [15, 16]. In realistic scenarios, all axes components of resistivity (x,y,z) are necessary to accurately detect this three-dimensional change over time. As seem in Ohm’s law, when an US pulse modulates the geometry of a tissue medium with inert electrical current flow, the resultant voltage changes and is observed on a high frequency (HF) scale. Depending on the current distribution geometry, *I*(x,y,z,t), the current densities, *J*(x,y,z,t), and the US pressure wave, *P*, deep brain signal maps over time can be made [3].

$$V_i^{AE} = -\iiint J_i^L \cdot J^I \; K\rho_0 \Delta P \; dxdydz \; (for > 100kHz)$$

Equation 2

The scalar product, $J_i^L \cdot J^I$, can be defined as the sensitivity of the AE detection electrode relative to the electrode lead field J_i^L. One ampere of current flowing through a recording electrode in a conductive volume is what defines the current distribution [17]. Due to vector summation, physiologic stimulating current vectors that are in the same direction to that of the lead field will project and affect the total V_i^{AE}[18]. To completely calculate the AE Voltage in a 3D medium, integrate the point spread function of the ultrasound function with the projected current densities onto each recording electrode’s lead field [18]. As seen in Figure 1, the current densities produced in the ex-vivo model emulate the innate physiological currents in the brain. Those signals are collected, noninvasively from the surface of the skull and transcranially pulsed with ultrasound to produce a voltage change.

Signal and Imaging Processing

Data that is collected in the normal AE scan is usually very noisy and not interpretable without processing. Data is processed in “fast time” (depth, or Z), “slow time” (real time scale), X, Y, repetition number, channel number. The collected data can be very noisy so multiple identical collections can be collected and averaged together to help remove some transient noise and is referred to as “repetition number”, or sometimes as “averages”. Data is then filtered along the fast time dimension by using the center frequency (0.6MHz) and bandwidth of the ultrasound transducer output by applying the fast Fourier transform to the data set and using a Hanning window on the data in the frequency domain and then transformed back into the time domain [24]. A Hanning window is used to filter the slow time (normal time) dimension by applying Fourier Fast Transform (FFT) to the slow time dimension, applying the Hanning window, and transforming it back to the time domain. The X and Y dimensions can be filtered using interpolation as well.

Gain and phase correction is performed with the in-lab developed processing software. The gain can be corrected by using the noise level for each channel as a baseline and importing gains that are known from our recording differential amplifier (*LeCroy* DA1855A). The phase shift is corrected by using a Hilbert transform around the peak magnitude point after the individual voltage vs. time data are spline interpolated. Then the magnitude of the cross-correlated data with a reference channel is used to determine the “Zero-Crossing Point” for the Hilbert transform algorithm. The resultant shift in data points allows shift that can be incorporated into a FFT for a more temporally accurate display for AE mapping [24].

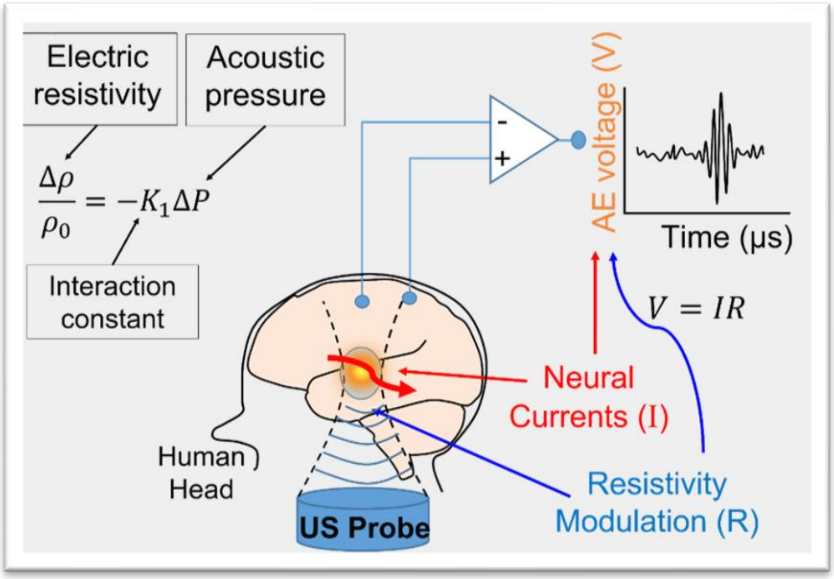

Figure 1: Change in electric resistivity is modulated by the introduction of changing US pressure wave which results in a HF detectable voltage (V_{AE}) [3]. Electric resistivity ($\Delta\rho$) is directly related to a tissue's interaction constant and the modulation of acoustic pressure (ΔP) from the US Transducer.

As a change over time this reconstruction can be illustrated in a cinematic to observe the locational change of the centroid of current propagation over time with magnitude and directional (polarity) components. In this research, the aim is to track that positional change relative to time and magnitude differences relative to stimulating current density size/format (dipole, monopole, etc.) in a real human skull phantom. Unlike ECG low frequency voltage (Equation 3), the interaction signal of AE high frequency voltage is spatially confined by the US focus wave (i.e., 0.15 – 1.5mm for 1-10MHz US transducers) collected in a forward propagation of the wave by a surface recording electrode (gold-cup in this scenario) [22, 23].

$$V_i^{ECG} = \iiint J_i^L \cdot J^I \;\; \rho_0 \, dxdydz \; (for < 10 \; kHz)$$

Equation 3

The complete mathematical analysis of the AE and ECG signal recording would be the summation of Equation 2 and 3 with a high and low frequency component. Limitations of AE detection model include in-band noise sources dependent on the testing environment and continues to compete with the target signal, but with correct hardware and software filtering the target signal is preserved. The summation of Equation 2 and 3 ultimately leads to Equation 4:

$$V_{AE}(X_1, Y_1, t_{us}, t_c) = -K\iiint (J(\mathrm{x,y,z},t_c) \cdot L(\mathrm{x,y,z}))\rho_0(\mathrm{x,y,z})\Delta\mathrm{P}(\mathrm{x} - x_1, \mathrm{y} - y_1, \mathrm{z}, t_{us})\mathrm{dxdydz}$$

Equation 4

V_{AE} is only non-zero when US pressure and electrical current are non-zero at the same time and location which leads to the wave packet confinement discussed earlier where the signal is dependent on the propagation US wave width [25]. As a result of such a small AE interaction constant, K, the V_{AE} is significantly weaker than the voltage from the lower frequency components.

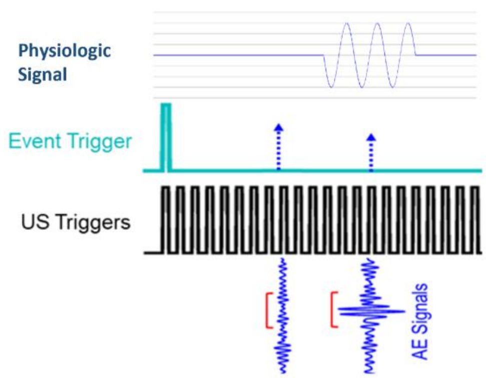

Figure 2: The "physiologic"/stimulus waveform consisted of 100-400Hz sinusoids with current magnitude 1mA-30mA enveloped within the shown square waveform. The example AE signals in blue indicate that a signal is created at the depth of current source (red bracket) when the stimulation is on but not when its off. The event trigger (light blue) indicates the start of each scan sequence and controls the feedback loop for stimulation and recording cycle. Many US pulses are sent (black) to increase the AE interaction effect and multiple the sampling effect [25].

Above (Figure 2) is a timing diagram that describes how the emulated physiologic stimulus, event trigger timing, the US trigger on an average AE Imaging scan. Each event trigger starts a feedback loop that consists of a stimulation profile, usually sinusoidal, however imported EEG-like waveforms have been explored as well in this work. These waveforms usually last no more than 50ms. Electrical AE and LF recordings are recorded up to 100ms. Depending on the type of scan performed, (M-mode, X-, Y-, XY scan) the sampling size is controlled using Matlab program user interface.

Root mean square (RMS) is a method related to standard deviation which illustrates the "power" of a signal or a more informative version to the concept of average amplitude of a signal [24]. Standard deviation is defined to represent how much of the data is some distance away from the mean:

$$\sigma = \sqrt{\frac{\Sigma(X_i - \mu)^2}{N}}$$

Equation 5

RMS is the measurement of data distance from a defined "zero" point (noise level).

$$RMS = \sqrt{\frac{\Sigma(X_i)^2}{N}}$$

Equation 6

Signal to noise ratio is defined in this work by the following equation:

$$SNR_{peak} = 20 * \log\left(\frac{Signal_{peak}}{Noise_{power}}\right)$$

Equation 7

$$SNR_{power} = 10 * \log \left(\frac{Signal_{peak}}{Noise_{power}}\right)$$

Equation 8

Equation 7 describes SNR in terms of peak signal whereas Equation 8 definition is in power metrics (dB).

Medical Need

In the past, experimentation included the use of simplified phantoms which mainly used saline and lacked certain geometrical similarities to the physiologic model. The use of gel center skull phantom with a multi-site electrode inserted allows for an excellent model to treat the medical need for a reliable imaging procedure when those who suffer from epilepsy have a corrective stimulator for intervention. Clinically, characterizing the pathways of neuronal current flow have been underdefined with EEG alone. To better characterize the spatiotemporal characteristic of the uncontrolled signal pathways in patients suffering from epilepsy, this tABI model is one step closer to noninvasively mapping a patient-specific neuronal current virtual diagnostic tool to eliminate unnecessary invasive procedures to offer patients a better quality of life. Transcranial acoustoelectric brain imaging (tABI) is an ultrasound-based method with the potential for greater spatial and temporal resolution imaging of current density distributions in the brain based on the acoustoelectric effect with the possibility of being non-invasive [5].

Thesis Aims

AIM 1: Develop applicable epileptic model for translational testing of clinical appearance of DBS/DE treated illness.

As stated before, epilepsy usually results in a specific region of the brain that has uncontrolled stimulation and results in local or global ictal pulses. Some questions include:

- Can I detect neuronal-like electrical signals through a human skull?
- Can I emulate the clinical treatment ictal model?

Luckily, we have access to a real human skull. This, combined with a conductive saline solution gel mold, helped with model development. Once embedded in the gel phantom, a multi-site electrode (DE/DBS) is stimulated to emulate deep neuronal-like current with temporal, spatial, and magnitude control. Additionally, direct comparisons of noninvasive AE detection method to the gold-standard EEG surface electrode (low frequency) detection method could be made.

AIM 2: Demonstrate noninvasive 4D tABI of time-and space-varying EEG-like currents generated by four contacts on DBS device implanted 30+ mm below the skull surface on the fine mm and ms scales. Create AE-Magnetic Resonance (MR) image cinematics to clearly describe the spatial and temporal variations in current to emulate that in a neural tract.

Not only was the physical phantom development set as a goal, but also determined a great comparative analysis and targeting system would be performed with the *BrainSight* motion tracking MR image system. Some questions I developed included:

- Can I use an MR image to assist in US transducer target determination and positioning?

- Can I use the virtual space in *BrainSight* to collect detection electrode leads and reconstruct the exact stimulation, US transducer and recording lead geometries?
- Can I overlay the AE cinematic over a collected brain phantom DE MR image and clearly display the current stimulation detection to the physical DE site locations?

MR image sequences were collected for the corresponding skull DE phantom prior to AE imaging procedure. They were imported into *BrainSight* and used to record experimental geometries for reconstruction after the imaging process. From there high contrast overlay cinematics showing both AE magnitude and polarity detection of stimulating currents as well as the DE physical geometries from the MR image were created.

AIM 3: Determine conduction velocities using peak AE voltage magnitude, site separability, and detection limits of AE signal in real skull DE model.

The DE and DBS models were used to easily control the geometry of the stimulation profile. Some questions included:

- Can I increase Signal to Noise Ratio (SNR) with known stimulating electrode geometries?
- Can I calculate current detection limits in a human head phantom?
- Can I reduce the number of surface recording electrodes needed to collect AE signal?

Using two different electrodes (*Spencer/AdTech* 12-site linear DE and *Infinity* 8-site concentric DBS) two basic models were created. One with the 8-site electrode in vertical orientation relative to the US z-depth axis and one with the 12-site electrode in horizontal orientation (anterior-posterior), perpendicular to the US z-axis. With these models have a physical, repeatable, clinically relevant model to determine the overall performance and accuracy of detection for the tABI method competitive with gold standard imaging techniques currently used. To ensure the method is within specification for clinical use, this work will address certain thermal and mechanical US effects as well as imaging goals.

The results for this work will include images and cinematics illustrating a hybrid modeling method (MRI/AEI) that has both anatomical Ultra Short Echo Time (UTE) MRI and electrical polarized information. In addition, peak negative pressure (PNP), Mechanical Index (MI), sensitivity scaled to peak pressure (μV/mA*MPa), root mean square noise level (RMS) (μV), noise equivalent current (NEC) (mA).

Chapter 2 – Protocol, Results and Discussion of Spatiotemporal Varying Current tABI Imaging in Human Head DBS Model

Methods

A. 4D visualization of current travel in human head model

A conductive solution (1.0% Agarose, 0.9% NaCl) was poured into a sealed human skull to mimic the brain for the head model. Starting from agarose powder, saline is added from adding 0.9% NaCl directly to deionized water. The mixture is heated until it reaches 80 degrees Celsius. While heating, intermittent stirring is needed to make sure the mixture stays in solution and the heat is distributed evenly. Once the solution is heated, wait until in returns to 40 degrees Celsius to pour into the specific mold needed for the experiment. Two separate head phantoms were produced with different stimulation geometries as well as a rectangular "heart" phantom that will be described with more in-depth discussion in the third chapter of this work.

Described below (Figure 3) is the first DBS electrode geometry used for a head phantom. In an almost arbitrary fashion, but mainly due to the ease of procedure, the electrode was placed in the skull phantom with very slight (< 10 degree) offset from vertical orientation. This meant the identification of specific sites on the electrode when there were multiple sites stimulated simultaneously would be much harder to differentiate due to the fact, X/Y scans were performed relative to the US transducer. There would most likely be shadow reflections along the Z-axis depth. Fortunately, the results yielded were much more fruitful due to the slight arbitrary angle to the point where multiple sites stimulated at multiple times are differentiable.

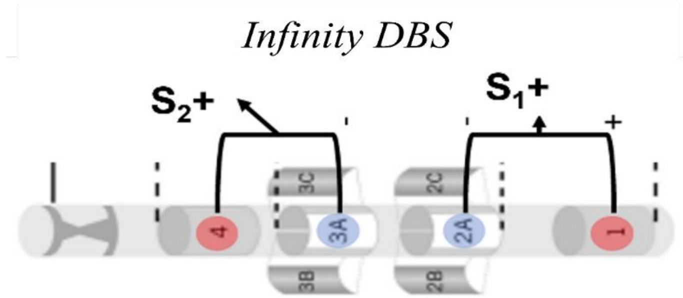

Figure 3: Infinity Deep Brain Stimulator (8-channel Infinity 6172ANS, Abbott Inc) shown with two dipoles (S1/S2). Red site is positive, and blue is negative stimulus. Sites have 2mm center to center separation.

A clinical deep brain stimulator (8-channel, *Infinity*, *Abbott*) was placed vertically in the gel with the tip approximately 30 mm from the skull surface (Fig 2). A multichannel stimulator (STG 4008 MTC) created two dipoles on four lead contacts carrying EEG-like waveforms (100-400 Hz bandwidth). Two gold cup electrodes (one on gel surface, one on left temporal skull) recorded acoustoelectric (AE) signals (Fig 4 and 5).

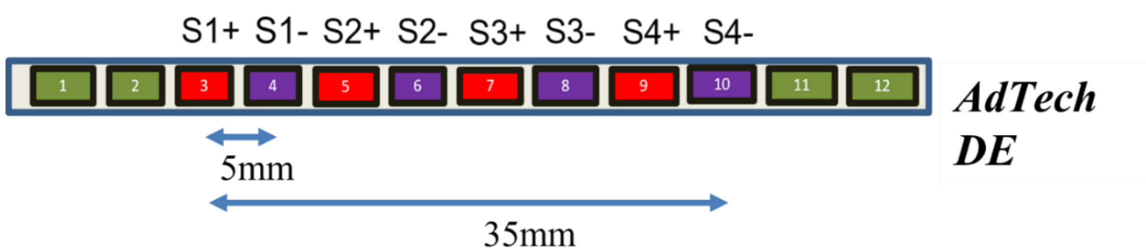

Figure 4: AdTech Depth Electrode (12-site, SD12R-SP05X-000) with four dipoles shown. Site separation is 5mm center to center, spanning 35mm range.

In a different head model, a clinical depth electrode (12-channel, *Spencer, AdTech Medical*) was placed horizontally in gel submerged 30 mm from the skull surface. Four monopoles or dipoles were created (Figure 4) using 3-cycle 200 Hz pulses generated by the multichannel stimulator. This model was much more effective at determining lateral site separation than the vertically oriented DBS. Multiple stimulation profiles were setup and tested from dipole to monopolistic and up to 4 dipole and 4 monopole setups during a single experiment. With the multiple site setup, the adjacent sites were stimulated sequentially or intermittently to validate whether the AE images could solve for the known temporal and spatial locations of their respective currents.

B. AE Signal Processing

AE High Frequency (HF) data collected by surface electrodes requires hardware and software filtering before it is displayed in a high contrast map. This work mainly involves the display of 4D mapping and tracking of these 4D (x,y,z,t) AE signals and how they vary over time. An A-Mode image in US diagnostics displays an amplitude with depth information [25]. This is usually created using a single piezoelectric US element. Depth values are gauged as a product of the time taken for the reflection to return to the transducer (pulse-echo) with the speed of sound through the specified medium (1480 m/s in water). An M-Mode image ("motion image") is a summation of multiple A-mode lines over time. M-mode images in "slow-time" (ms) are created and amplitude which can be displayed as a 2D image vs time. B-mode images are created with a 1D or 2D US transducer.

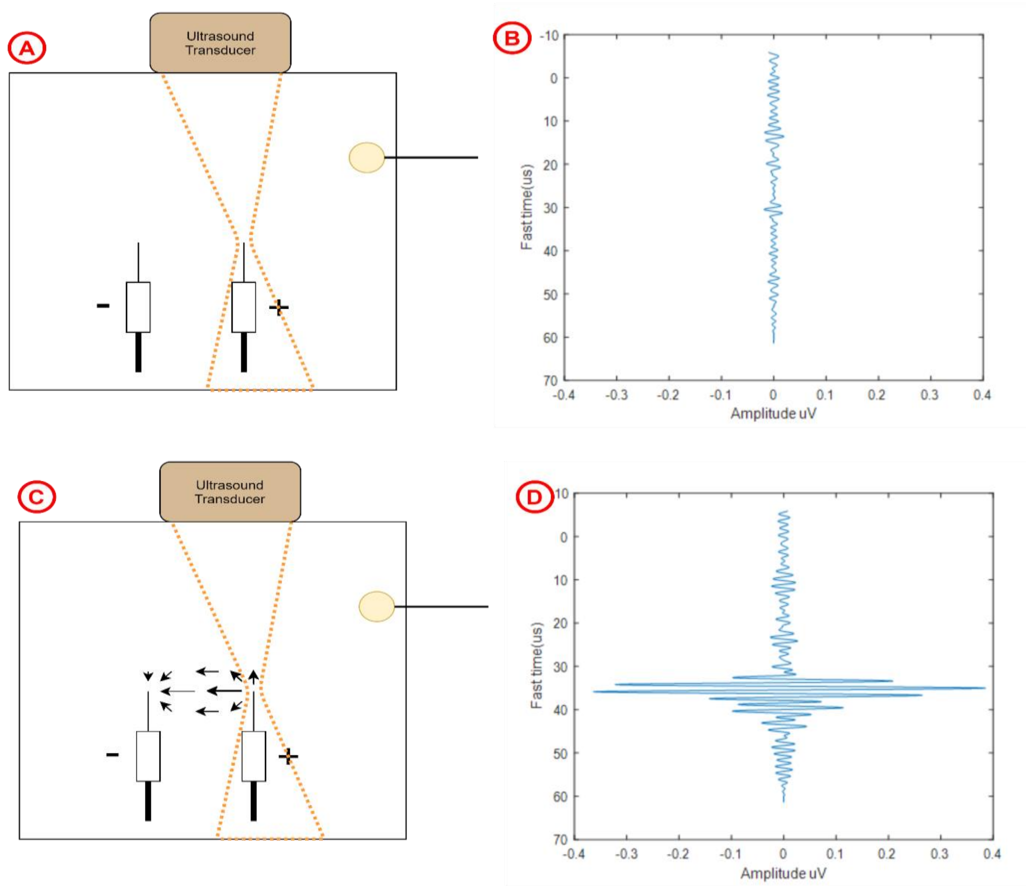

Figure 5: AE signal induced and recorded on gold cup electrode. [A] Diagram shows saline bath with two stimulating electrodes without any current. The ultrasound beam is focused on the positive (+) stimulating electrode. The gold cup picks up any voltage within the bath as is shown in [B]. When Current is injected into the bath[C] the gold cup electrode senses the AE voltage[D] induced by the interaction of the ultrasound beam and the current gradient within the beam focus [24].

The US elements are phased such that the US focus is raster-swept along an elevation (i.e., *x*, *y* at fixed *z*-depth) [25]. C-mode images are images with 3-directional raster scan components (*x*, *y*, *z* over a period *t*). The final images in this work are all C-mode images with polarity components to current travel. Another major difference between traditional US (pulse-echo) and AE imaging is that pulse echo is a send-receive communication whereas, AE imaging is only a forward process then collected as a voltage from a nearby sensing electrode. Once the AE magnitude C-mode images are created, cinematics were created that can be overlayed onto MR images that show the electrode structure for referential location. As seen in Figure 5, if the ultrasound beam interacts with a non-stimulated electrode (A), no AE voltage will occur (B). However, when there is either physiologic current or artificially emulated current (C), an AE voltage will be produced and result in a measurable signal (D).

C. BrainSight and Armature US Targeting System

A 0.6 MHz 2D US array steered a focused US beam through thick skull to generate tABI maps proportional to the local current densities. Verasonics system was used to pulse the US transducer at 4000Hz with voltage output of ~1.6MPa. From here, raster scans are made with targeted focus scans using a "chirp" pulse. Each pixel is recorded with at least ten averages, then the scans are recompiled using Matlab based signal processing programs. The stimulation profile was controlled by a multichannel stimulator (STG 4008). This stimulator has the capacity to run 8-channel dipole stimulation profiles in any sequence. This was key in creating time-varying stimulations in the models. Matlab user interface controls signals were sent to the "din" connector DBS/DE.

Firstly, calibration of the H235 (0.6MHz) 2D US transducer to *BrainSight* program is necessary to coordinate the virtual axis system to the "real" geometries present in the experiment. When the US transducer has been correctly calibrated, positioning, and orthogonal targeting of the desired stimulation site can be displayed real-time which is ineffably helpful for targeting scans. With this feature accuracy of scans within 1mm error from real life geometries are realized. Prior to performing an AE scan, a position capture protocol was performed to correct for any offset with the actual skull and the previously captured MR image. This process consists of pointing and sampling predetermined markers set on the surface of the skull ("donut" shapes in Figure 6). *BrainSight* includes a motion capture camera which tracks a specified pointer that facilitates this calibration process. After calibration of the markers, AE recording electrodes can be placed on the surface of the skull (usually gold cup) and calibrated using the same pointer used for the donut markers. With these marker inputs a completely virtual reconstruction of the AE hardware experimental setup combined with the MR image BrainSight setup is created. With this an MR 3D UTE sequence reconstruction to compare and overlay with 4D AE detection maps can be used for anatomical reference.

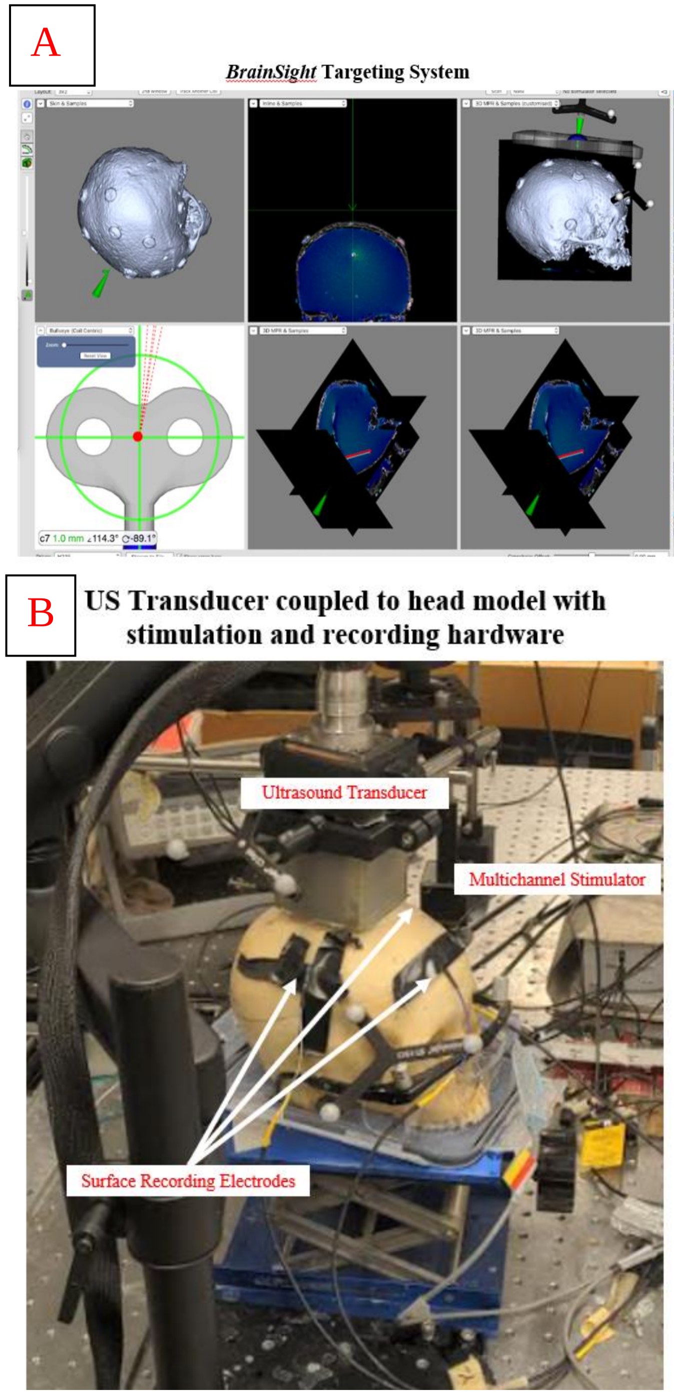

Figure 6: User interface for imported Magnetic Resonance (MR) image of head phantom to assist with US targeting of stimulated area (A). Photo of US transducer coupled to head model phantom with agarose gel inside stimulated with DE (B).

Three noninvasively placed recording gold electrodes were used in a triad (frontal, left-parietal, right-parietal) (Fig 6 and 7). Utilizing MR imaging (MR, 3T, *Siemens*), the *BrainSight* neuronavigation targeting system facilitates efficient positioning of the US transducer to focus on a target area near the stimulation contacts emulating neuronal activation. The 12-site depth electrode produced a wide geometry to scan for field of view (35mm) and accuracy with proximal platinum sites (Fig. 4). 2.5MHz low-pass filters on AE recorded signals as well as apply 4x gain to the signals through in-house developed pre-amplifier hardware. The processing of signals is performed using Matlab programming environment to reconstruct 3D images and 4D movies for signal analysis.

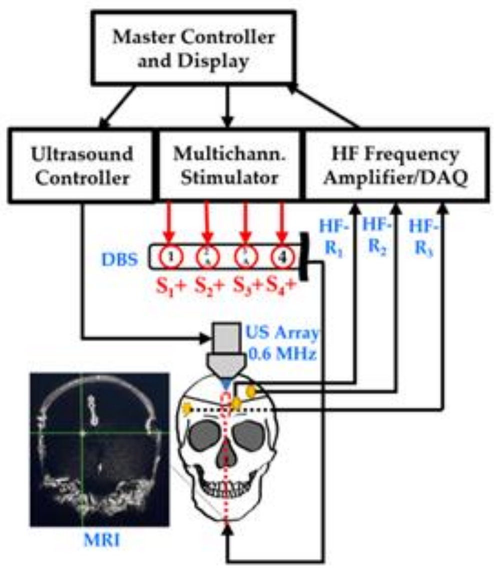

Figure 7: MR Image with top-level experimental hardware organization. 4-site stimuli shown with coupled 0.6MHz US transducer. Three HF recording electrodes shown to help with BrainSight MR image overlay geometry with recorded. Recording and filtering Data Acquisition (DAQ) system used to capture three signal inputs for post processing and display purposes.

As seen in Figure 7, there are three main systems involved in stimulating neuronal-like currents, producing the AE effect, and recording that resultant signal. The stimulator (STG 4008) is directly connected to the DBS/DE implanted in the skull to produce detectable signal. The H235 US transducer sends the interacting pressure wave through thick skull to interact with the latent currents and finally the Data Acquisition hardware collects and filters the LF and HF data into respective files. The LF data will be used to verify the phase and gain validity of our collected, novel, HF AE voltage signal. The hardware we use is a National Instruments (NI) PXI-5105 and PXI-6289 signal acquisition system. The stimulation hardware can introduce a myriad of stimulation profiles into the model including, EEG-like slow waveforms (i.e., alpha, beta, gamma, delta), simultaneous polarized signals, as well as, recorded ictal signals. Acoustic coupling between the skull and the transducer must be preserved using coupling gel. One of the major issues with the current testbed is maintaining consistent contact of the recording electrodes to the surface of the skull and eliminating noise with a true ground source.

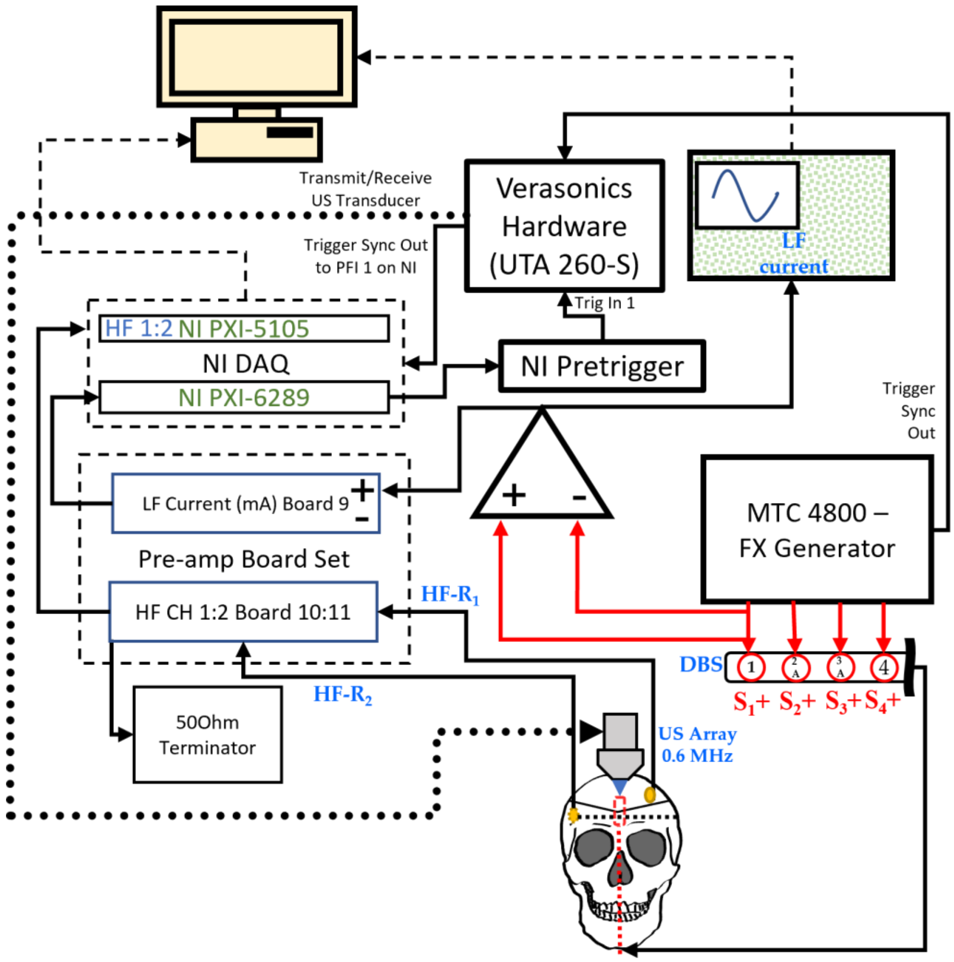

Figure 8: Above is a comprehensive hardware diagram explaining the pathway of the stimulation and recording models. The DBS is shown with 4-dipole connections to the head phantom. The H235 0.6MHz 2D US array is affixed transcranially to the skull with US saline gel. HF recording gold cup electrodes (HF-R_1, HF-R_2) trace from the skull surface to the Preamp board (prototypical filter made in-house) into two channels where HF and LF signals are split. LF current from a diff-amp (measured across 1Ω resistor not shown) is input into another filter board and all signals are taken into National Instruments DAQ and displayed for software processing. Verasonics hardware (UTA 260-S) facilitates US power and trigger regulation feedback loop. BrainSight hardware not shown.

As seen in Figure 8, the present hardware setup for experimentation is complex and has room for consolidation. However, the procedure is repeatable and has specific application to clinical scenarios regarding electrical brin disorders. The LF current can be easily displayed on an oscilloscope or on a single display with Matlab software processing and NI DAQ controls via network connection (ethernet hub). LF current is recorded for control (differential voltage measurement → Amperage) and collected for comparison to gold cup surface LF EEG and HF AE voltage target signal.

Results

Results collected from the detection system are unlike many other physiologic signal detection scenarios. ECG and EEG traditional waveforms detect low frequency signal, while the AE signal is much higher frequency meaning there are many interfering, in-band noise sources that need to be eliminated to rectify the target signal. Noninvasive 4D tABI of time-and space-varying EEG-like currents were generated by four contacts on DBS device implanted 30+ mm below the skull surface on the fine mm and ms scales. Spatial and temporal tABI movies were analyzed to determine spatial separability of the contacts, resolution, and current detection limits through the skull. These signals overlapped in time as to simulate a travelling wave that changed physical location with time. Another factor in need of definition was the extent to which simultaneous signals with opposing polarities would be detected with tABI compared to the low frequency (LF) detection method such as EEG. TABI maps at individual pixels were highly correlated with either (or both) the S1/S2 current waveforms, and the LF EEG recorded simultaneously (Fig 9, 10).

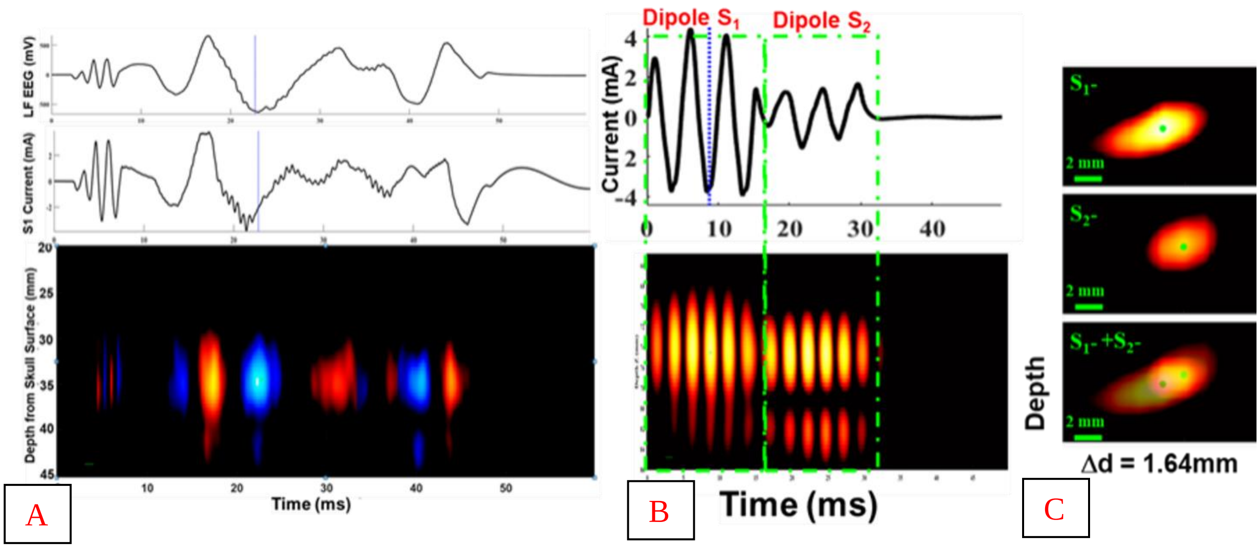

Figure 9: (A) 1st Stimulation scenario with vertically positioned DBS: EEG-like waveform with variable frequency profile stimulated with two dipoles on Infinity DBS. (B) The time separation between site stimulation is shown by with dashed-green boxes for each separate stimulated dipole. (C) Platinum site separation of 2mm (center to center) was visualized with Δd = 1.64mm.

As seen in Figure 9, two dipoles were stimulated with a separation of 2mm contact spacing on the *Infinity* DE. Varied EEG-like waveforms were introduced into the phantom. These dipole signals were timed at the same time, however, in another stimulation profile the timing of the signals were staggered in time. Dipole S1 was initiated at t = 0ms and ended at t = 15ms. Dipole 2 was initiated at t = 15ms and ended at t = 30ms. After observing the resulting EEG signal, a resultant sinusoid occurs continuing from t = 0 to t = 30ms with a reduction in signal because of the EEG LF electrode placement relative to stimulation. On the contrary, the AE HF result (seen in right Figure 9) shows a clear change in signal centroid location of ~1.64mm. This was very close to the actual value of the site separation (2mm).

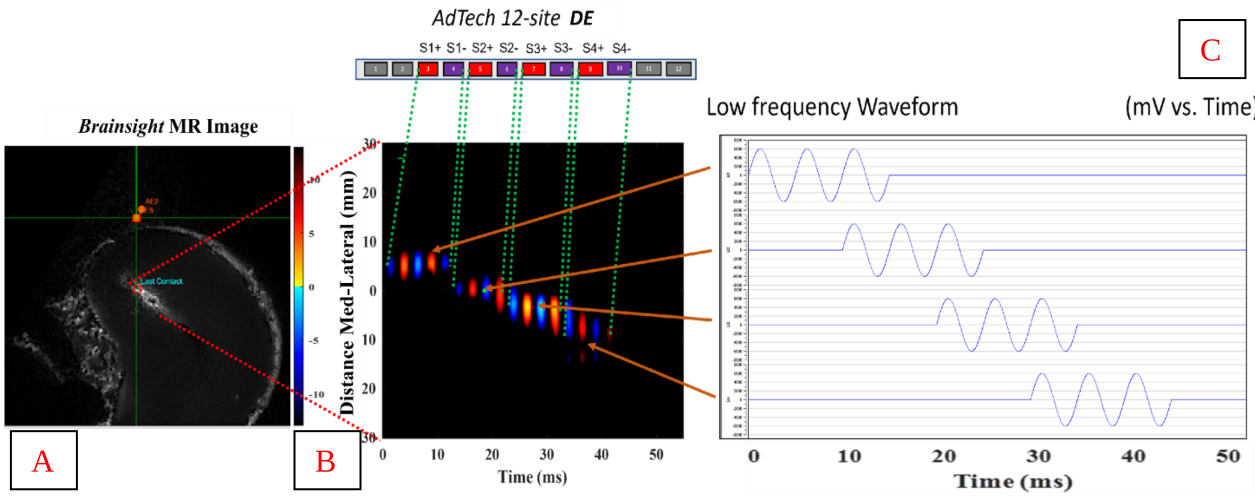

Figure 10: 2nd Stimulation scenario using the AdTech 12-site Depth Electrode placed anterior-posterior ~30mm deep from the skull surface. (A) Imported MR images (UTE sequence for enhancing skull contrast) presented here. (B) An exploded view of the detected AE voltages to visualize a transverse horizontal line at 30 mm below the skull surface over stimulation time in msec is shown. The AE polarized image shows the 4 separate locations of stimulation (S1-S4) at varying times each separated center-to-center ~5mm. (C) The LF waveform shows four equivalent three-peak sinusoids corresponding to the four dipoles stimulated on the depth electrode.

In the second setup using the *AdTech* DBS (12-site), 4 dipoles were stimulated with temporally and spatial variations. Each dipole, center-to-center, are separated by 5 mm. The DBS transverse the horizontal anterior-posterior axis (z = 30mm below skull surface) with sinusoids lasting 15ms on each consecutive site. To emulate a travelling wave the signals were temporally staggered with an overlap of 5ms. Assuredly, this would in theory result in a convolved signal if detected with solely LF EEG and the polarity of the adjacent dipoles were the same. In the AE image analysis (Figure 10) clear temporal and spatial separation exists along with base banded polarity at the separated stimulation sites. The site separations were 4.64mm on average from adjacent dipole to dipole (actual center-center spacing = 5mm).

Our analysis methods for creating these AE images and movies include the use of Matlab programs with reconstruction filtering. These methods include determining parameters such as Signal to Noise ratio (SNR), correlation between LF/HF channels and spectrum intensity mapping of magnitude with polarity components.

SNR in the experiments was calculated using absolute known AE signal and comparing this to the noise level. One method of calculating SNR is solely determined by the amplitude of the signal while another technique includes a relation between the power of the signal and that of noise combined in a logarithmic fashion. A region of image is sampled that has a well-established noise level and compare that to a well-established region of true AE signal level. After reconstruction of the images and correction for gain and phase, some assumptions are made while also correcting for other variables. It is assumed that the noise levels are common mode where the noise levels experienced on all hardware are similar. The phase correcting algorithm used for display of all channels due to temporal shift includes [24]:

1. Create array of A-line data from same slow time and scan point
2. Interpolate A-lines with spline to smooth data and increase resolution of shift
3. Determine peak signal from data and include "cushion" without noise sample
4. Hilbert transform A-line data for all channels and cross correlate each channel with a reference channel
5. Determine cross-correlation magnitude.
6. Use magnitude to determine "zero-crossing point" relevant to the phase of the Hilbert transformed data.

For more in depth analysis of this analysis procedure please reference source [24].

Shown below is the focused A-line waveform on a single recording electrode from the second *AdTech* 12-site electrode study. The slope from the second graph (Figure 11) shows how the detected AE signal in µV relates to the stimulated LF signal magnitude in mA.

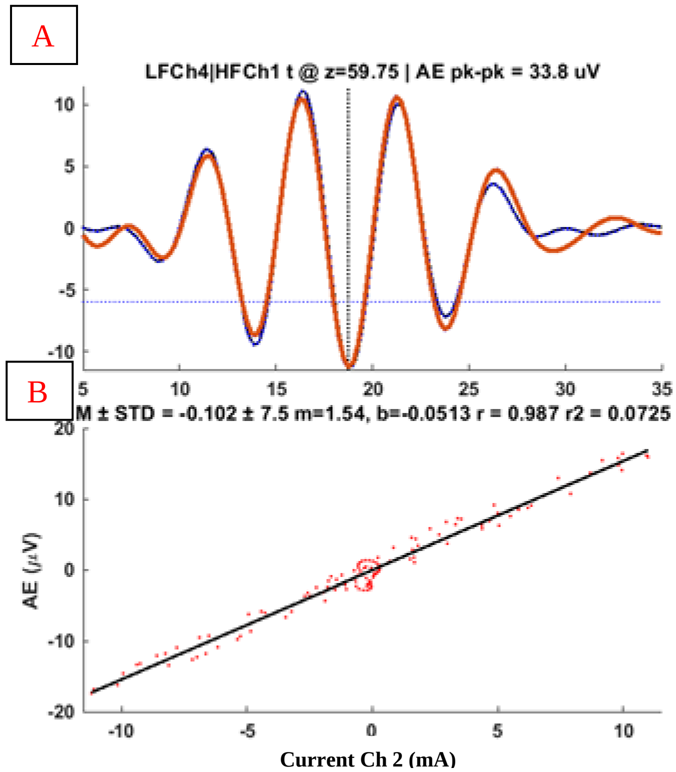

Figure 11: (A) Low frequency (Orange)/High Frequency (Blue) recorded signal amplitude pk-pk (mA) over time. (B) Signal sensitivity (AE voltage vs. Low Frequency mA) of detected signal versus actual injected signal is extracted. A slope of 1.54 µV/mA is calculated.

From the above image (Figure 11) and pressure calculations collected through the skull using a calibrated 1mm ultrasound hydrophone (*Precision Acoustics*, Dorchester, England), the sensitivity is scaled to PNP (@ 35V H235 2D US transducer output → 0.78MPa) as 1.97 mA*MPa. The MI was <1 (0.859). RMS noise level was calculated at 0.67µV for a dipole through the skull and an AE power SNR of 39.21dB.

Discussion

There is high correlation between the LF and HF signal timing which proves sensitivity to the AE signal where the EEG LF signal would be present, however, AE images provide much better 3D information. Some of the other goals achieved include:

- Conduction velocities tracked from centroid magnitude (x,y,z) over time which varied both temporally and spatially to better emulate a real in-vivo testing scenario
    - *AdTech* electrode was 4.71 m/s, and the *Infinity* DBS was 3.9 m/s
- Mapped specific 1.5mm and 4.5mm site separation on *Infinity* and *AdTech* electrodes, respectively, spanning wide field of view (35mm) at sub-cranial depth of ~30mm on both agarose/saline gel models
- Detection limits were nominally found to be ≤300µA with stimulation of LF current at levels varying from 1mA to 30mA
- RMS noise level for recorded signals was found to be 0.67µV.
- Detection of opposing polarized adjacent signals that would cancel to net-zero magnitude with normal EEG surface detection but were preserved with single electrode AE surface detection.

Better sensitivity is expected with monopolistic stimulation because current source density will be much higher and spatially concentrated. The dipole setup was interesting however, because varying LF current pathways were established that leave room for exploration in future studies (i.e., electrode site "crosstalk", far-field monopole "sink" detection and polarity studies). Reconstruction of adjacent opposing polarity signals that would normally cancel because the adjacent sinusoids are of opposite polarity (i.e., the derivative of the sinusoids were opposing and therefore when convolved would result in net zero) were preserved with AE imaging analysis. With the tABI technique these travelling waves will be preserved regardless of the vector location, unlike EEG surface electrode detection techniques where this would most likely be invisible.

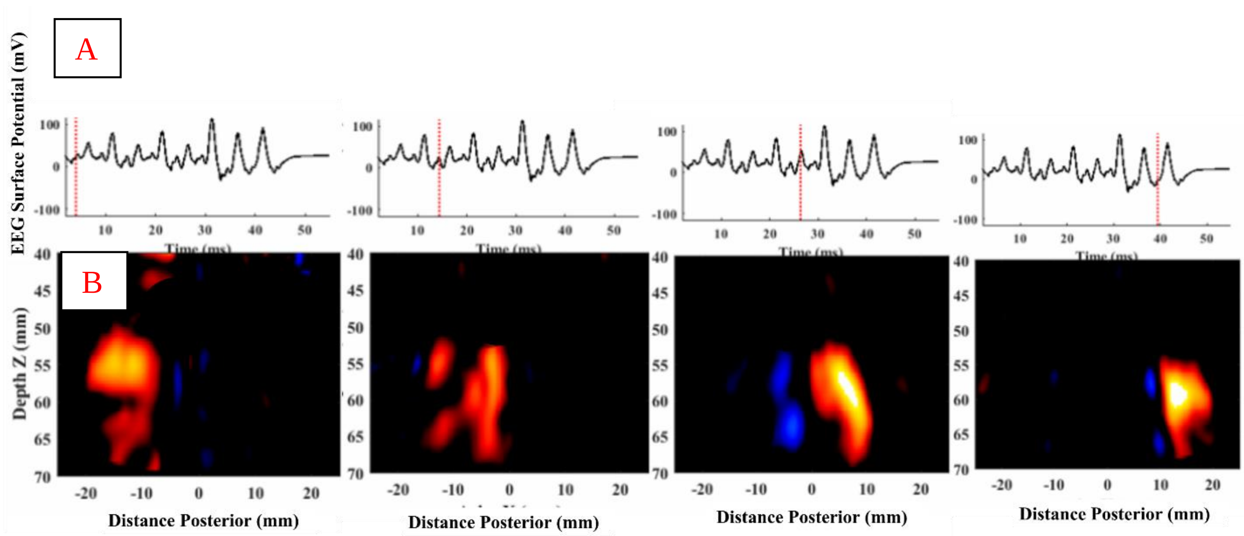

Figure 12: Because a cinematic cannot be inserted into this document, here is a frame-by-frame process with the red dotted line on the (A) A-line EEG surface trace for time reference. (B) Below the EEG traces the corresponding AE images are mapped with baseband, and the location of the central peak magnitude changed as time continues. This change is relative to the travel of current from S1-S4 dipole locations. The A-line EEG detection above these maps proves this deep brain signal (~30mm) cannot be rectified in the same manner, resolution, accuracy that tABI noninvasive spatiotemporal mapping offers.

As shown above (Figure 12), the travelling signal stimulated on the four dipole sites cannot be illustrated with EEG LF surface detection. The clarity of tABI technique for deep brain, noninvasive mapping of spatiotemporal travelling currents is peerless with applications for epilepsy and many other electrical brain disorders.

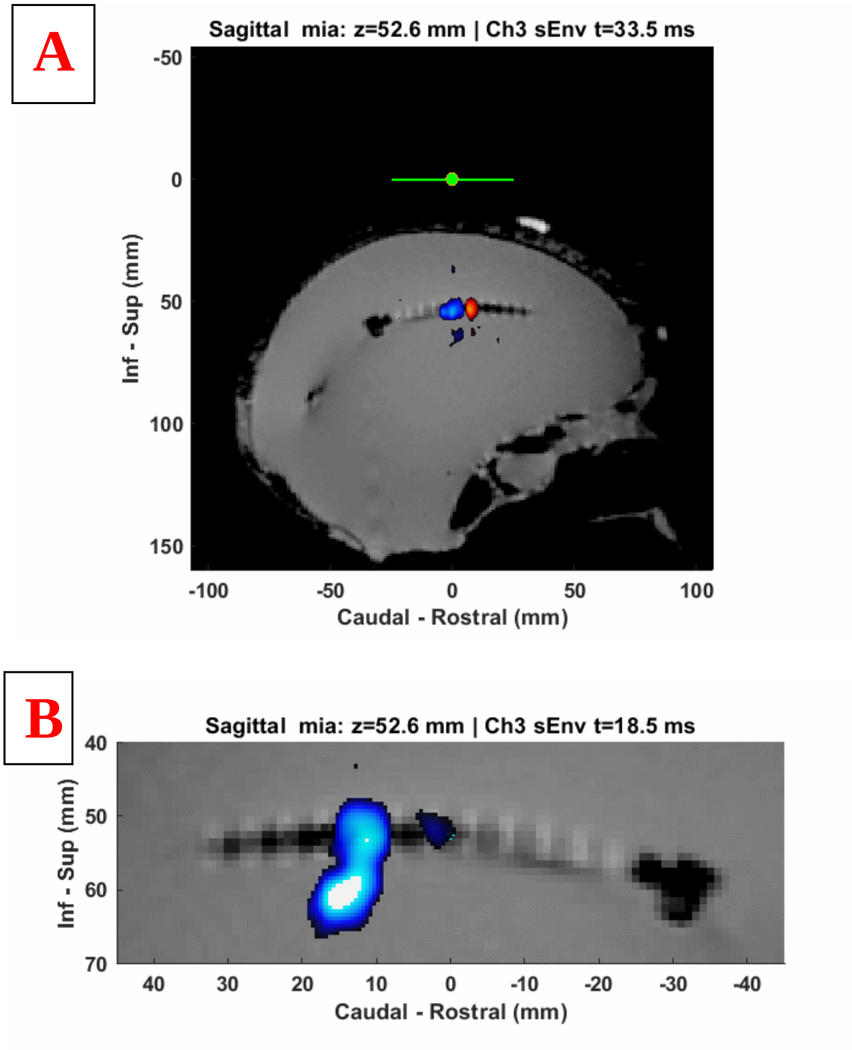

Figure 13: (A) Frame of cinematic overlay displaying result of tABI image travelling along the implanted DE. Underlay is sagittal view of MR image taken of skull phantom. (B) Zoomed view of same DE with tABI signal overlayed on MR image from BrainSight. UTE MR sequence used in these figures.

These overlay movies shown above (Figure 13) for model named "Mia", prove that the model can effectively assist with diagnosis on a translational level comparable to EEG if not better with higher accuracy and deep brain penetration while remaining non-invasive. The next move will be to streamline the hardware setup to fewer devices: Stimulator, Recorder, Filter, Display. A more pressing next step would be to translate these overlays into a 3D vs. time movie that can be rotated with a user interface that allows radiological manipulation like other translated imaging methods.

Chapter 3: Conclusions with Epilepsy Study and Future Work Toward Applicable Cardiac Model

Conclusion

Results from this work can be classified in two categories: qualitative and quantitative. Many of the goals set for this work were met, but there remains work to expand these models and the process behind methods. The goal of developing an applicable epileptic model for translational testing of clinical appearance of DBS/DE treated illness was a success with the ex-vivo skull model, *BrainSight* MR imaging program, and tABI spatiotemporal neuronal current tracking system. *Can I detect neuronal-like electrical signals through a human skull? Can I emulate the clinical treatment ictal model?* Yes, with both the ex-vivo and in-vivo swine model there is proof that neuronal-like signals can be detected and mapped using the tABI method. The second aim of demonstrating noninvasive 4D tABI of time-and space-varying EEG-like currents generated by four contacts on DBS device implanted 30+ mm below the skull surface on the fine mm and ms scales and creating AE-Magnetic Resonance (MR) image cinematics to clearly describe the spatial and temporal variations in current to emulate that in a neural tract was met. The next step in development of these cinematics is creating a manipulatable 3D over time model that can be analyzed similarly to a 3D MRI scan in traditional radiology.

MR image sequences were collected for the corresponding skull DE phantom prior to AE imaging procedure. They were imported into *BrainSight* and used to record experimental geometries for reconstruction after the imaging process. From there high contrast overlay cinematics showing both AE magnitude and polarity detection of stimulating currents as well as the DE physical geometries from the MR image were created.

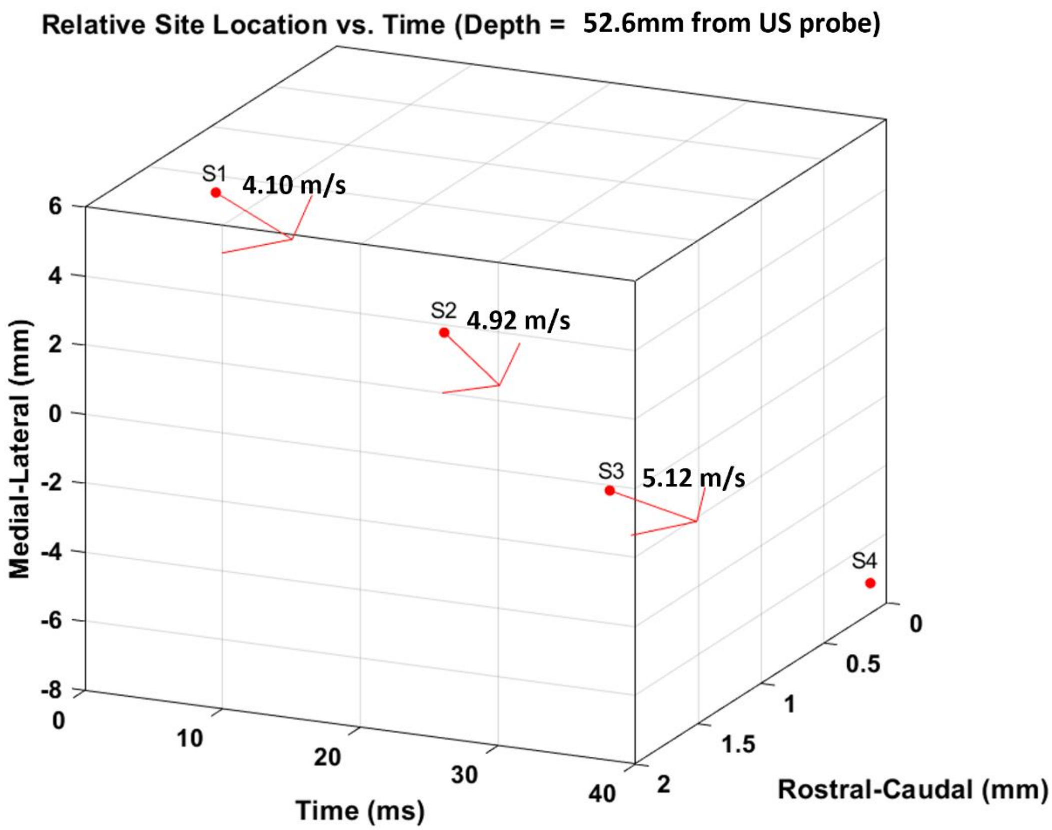

Figure 1414: Plotted above is relative location map of the tracked signals on sites S1-S4 of the AdTech Depth Electrode. The arrows indicate the vector path of travel with their relative velocities.

Conduction velocities were determined using peak AE voltage magnitude, site separability, and detection limits of AE signal in real skull DE model (Figure 14). Quantitatively the velocity measured between sites through AE image analysis on the *AdTech* depth electrode was 4.71 m/s and the same for the *Infinity* DBS was 3.9 m/s. These values were calculated through subtracting the spatial distance between the peak activation at each site and dividing the difference by the time interval, please reference Figure 14. Interestingly, the velocity between sites for the wider contact to contact length (5mm on the *AdTech* electrode) seems to be faster than the closer contact width (2mm on the *Infinity*). The SNR continues to be a major complication with our setup with in-vivo experiments. There is a significant amount of in-band noise that interferes with our target signal with swine surgeries which we have not been able to emulate with ex-vivo experiments. There are designs for a passive and active filtering electrode in prototypical phases to assist with this noise reduction. Ideally a large quantity array of surface electrodes would help with our signal detection accuracy and focus.

With these models, there exists a physical, repeatable, clinically relevant model to determine the overall performance and accuracy of detection for the tABI method competitive with gold standard imaging techniques currently used. To ensure the method is within specification for clinical use, this work addresses regulatory thermal and mechanical US effects as well as imaging goals for tracking spatiotemporally varying electrical currents.

Outside of ex-vivo modelling, induced ictal currents were recorded using LF techniques on the swine model with some success (Figure 15). TABI 4D visualization of grand-mal seizures of anaesthetized swine have helped us to see the imminent possibility of clinical use for an effective epileptic imaging technique.

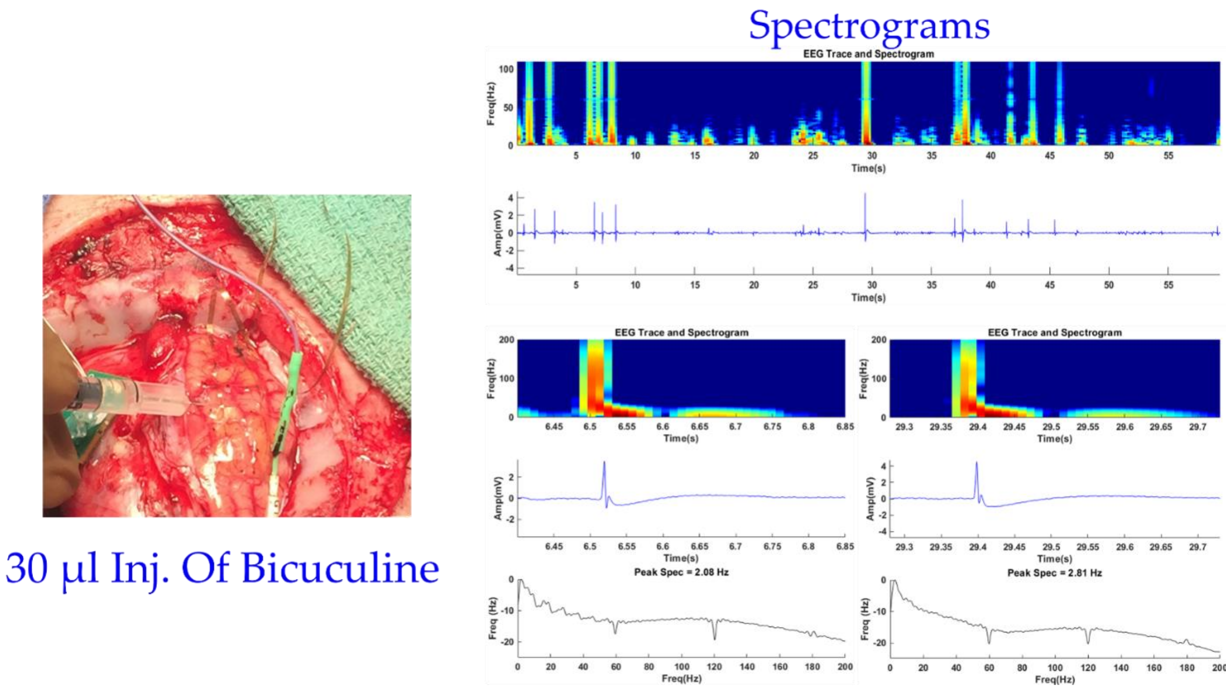

Figure 15: Sample of in-vivo acute swine studies using bicuculine injection to induce ictal pulses and measure the resultant neuronal reaction. These seizures are global and can help us to continue in development of the swine model and lead into more chronic studies of LF waveform mapping to better understand and diagnose epilepsy in the human model.

The move from ex-vivo to in-vivo study will illustrate the efficacy of the imaging technique for noninvasive techniques for possible other diseases such as Multiple sclerosis or Alzheimer's disease.

Future Work: Cardiac Ex-Vivo Model

AIM: Create a reproducible ex-vivo model that emulates the physiologic, anatomical, and electrical characteristics of a human heart to characterize spatiotemporally varying currents to assist in diagnosis of AF.

Using similar 3D printing and DBS/DE stimulation methods a model was developed alongside that of the tABI spatiotemporal travelling wave model that would assist in the diagnosis of irregular cardiac electrical activation.

Acoustoelectric Cardiac Imaging (ACI) was used to develop the first real-time electrical cardiac mapping system based on disruptive acoustoelectric (AE) technology. ACI could achieve accurate, real-time, volumetric images of current densities in the human heart with mm and ms resolution. The patented technology, developed by Dr. Witte at The University of Arizona will be the foundation toward product realization at ElectroSonix LLC. Below (Figure 16) is the original theoretical design behind separation of the QRST wave into its deconvolved components in effect to monitor a travelling wave in space over a wide field of view.

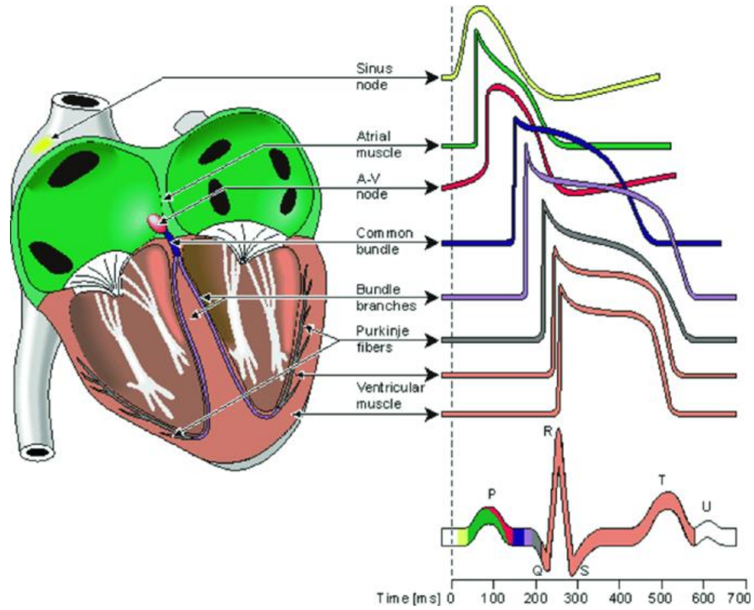

Figure 16: Action Potentials and how they anatomically vary; in summation the result is a QRST wave. To better emulate the spatiotemporal travelling of the cardiac current a model was created using the Infinity DBS with 8 sites.

The figure below shows an original 3D design that has yet to be built but offers a model for implanting a Depth Electrode (diameter 1.5mm) into a mold of agarose/saline solution that mimics the cardiac conductive tissue and has an insulative shell surrounding for US transducer connectivity. In this model, the goal was to stimulate relevant waveforms (see Figure 16) to each of the colored sites to map the flow of current through the anatomy of the heart.

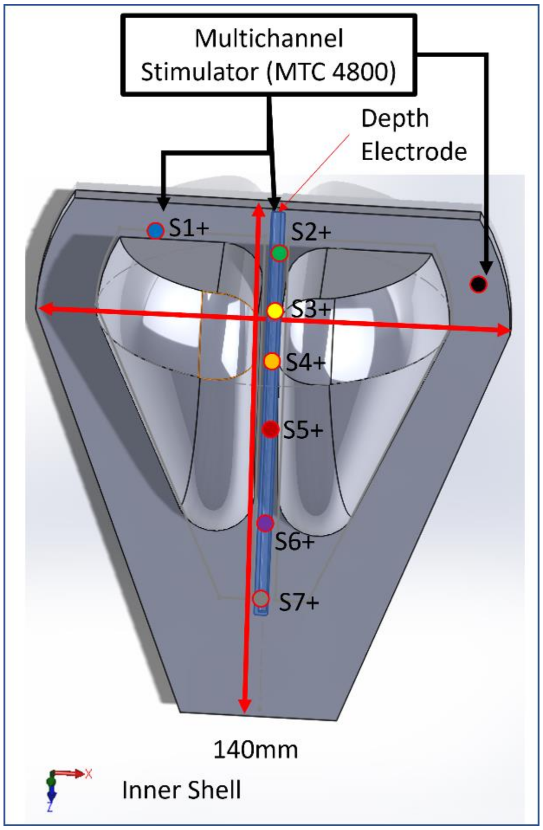

Figure 17: Above is the first design for a cardiac electrical model with an embedded DBS Infinity electrode. This design was never made and has potential to be a future step. The different sites correspond to Figure 16 and the respective QRST components. The design that was implemented was a simpler version of this model. This model had an electrically insolated controlled current path that emulated the geometry of the cardiac muscle.

As a steppingstone, the below model was developed (Figure 18) which includes an agarose/saline mixed gel interior with a thick humimic ballistic plastic on the exterior. Inserted in the agarose conductive gel was the same 8-site *Infinity* DBS used in one of the previous head skull phantoms. In a similar fashion to the head model, stimulations of small amounts of current were introduced into the gel with the US transducer affixed to the ballistic insulative mold.

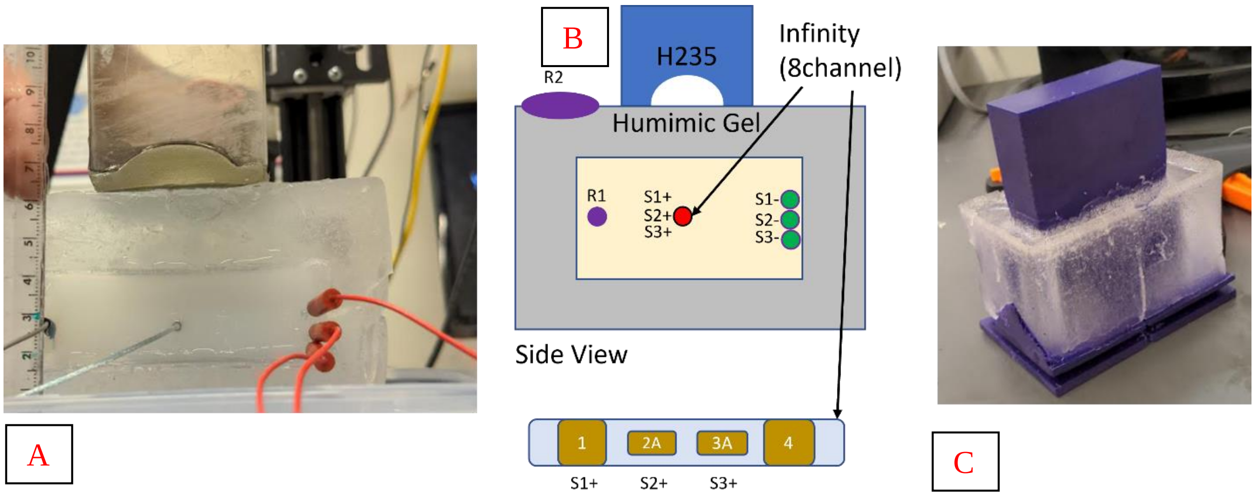

Figure 18: Above is the experimental setup for the first iteration of the cardiac travelling current model. (A) The US Transducer (H235 0.6MHz) is seen affixed to the side of the model with the Infinity DBS in parallel with the long axis (y-axis) of the 2D probe. (B) The stimulation profile included 3-monopoles (S1-S3) with "sinks" in far field (middle green dots). Sites 1, 2A, and 3A were used on the DBS electrode (bottom middle). (C) The ballistic humimic insulative gel mold was made with a 3D printed form.

Collecting AE signal from this model (Figure 18) with a monopolistic stimulation setup and a single gold cup electrode affixed to the gel was a success. This model needs to be further tested to better emulate what was incepted in Figure 16. This serves as an excellent place for the continuation of a travelling current Transthoracic Acoustoelectric Cardiac Imaging (tACI) model.

References

[1] Mandal, Pravat K et a l. “A Comprehensive Review of Magnetoencephalography (MEG) Studies for Brain Functionality in Healthy Aging and Alzheimer's Disease (AD).” Frontiers in computational neuroscience vol. 12 60. 23 Aug. 2018, doi:10.3389/fncom.2018.00060K.

[2] Stolk et al., “Integrated analysis of anatomical and electrophysiological human intracranial data.” Nature Protocols, 2018.

[3] Witte et al., “In Vivo Swine Model of Focal Seizures for Developing and Validating Acoustoelectric Brain Imaging of Neuronal Currents” National Institutes of Health Brain Initiative, 2022. (poster).

[4] Centers for Disease Control. Types of Seizures - Epilepsy. 2021. website. 2022. https://www.cdc.gov/epilepsy/about/types-of-seizures.htm.

[5] Barragan A, Preston C, Alvarez A, Bera T, Qin Y, Weinand M, Kasoff W, Witte RS. Acoustoelectric imaging of deep dipoles in a human head phantom for guiding treatment of epilepsy. J Neural Eng. 2020 Oct 30;17(5):056040. doi: 10.1088/1741-2552/abb63a. PMID: 33124600; PMCID: PMC8167191.

[6] A. Alvarez, C. Wilhite, C. Preston, T. Trujillo, A. McArthur, D. Mustacich, R.S. Witte. “4D Cardiac Activation Wave Mapping in In Vivo Swine Model using Acoustoelectric Imaging.” Institute of Electrical and Electronics Engineers (IEEE) International Ultrasonics Symposium. Glasgow, Scotland. October 2019.

[7] A. Alvarez, C. Preston, T. Trujillo, C. Wilhite, A. Burton, A. Barragan, C. Ingram, R. S. Witte. "Mapping Cardiac Electromechanical Coupling using Acoustoelectric Echocardiography." American Medical Association (AMA) EXPO Research Poster Competition. San Diego, CA. November 2019.

[8] A. Alvarez, C. Preston, T. Trujillo, C. Wilhite, A. Burton, A. Barragan, C. Ingram, R. S. Witte. "Mapping Cardiac Electromechanical Coupling using Acoustoelectric Echocardiography." American Physician Scientist Association (APSA) West Regional Meeting. Loma Linda, CA. November 2019.

[9] Allard, M., Preston, C., Huang, C., Chen, N. K., & Witte, R. S. (2021). Neuronavigation with Skull Segmentation and Acoustic Modeling for Guiding Transcranial Acoustoelectric Brain Imaging. IEEE International Ultrasonics Symposium, IUS. https://doi.org/10.1109/IUS52206.2021.9593472

[10] Preston, Chet et al. "High resolution transcranial acoustoelectric imaging of current densities from a directional deep brain stimulator." Journal of neural engineering vol. 17,1 016074. 27 Feb. 2020, doi:10.1088/17412552/ab6fc3.

[11] Alvarez, Alexander et al. "In vivo acoustoelectric imaging for high-resolution visualization of cardiac electric spatiotemporal dynamics." Applied optics vol. 59,36 (2020): 11292-11300. doi:10.1364/AO.410172

[12] J. S. Duncan, G. P. Winston, M. J. Koepp, and S. Ourselin, "Brain imaging in the assessment for epilepsy surgery," *Lancet Neurol.*, vol. 15, no. 4, pp. 420–433, 2016, doi: 10.1016/S1474-4422(15)00383-X.

[13] Pavlov I 1927. Conditioned Reflexes: An Investigation of the Physiological Activity of the Cerebral Cortex. (London: Oxford University Press) (1927).

[14] Lilly J C and Cherry R 1954. Surface movements of click responses from acoustic cerebral cortex of cat: leading and trailing edges of a response figure J. Neurophysiol. 17 521–32 (1954).

[15] Q. Li, R. Olafsson, P. Ingram, Z. Wang, and R.S. Witte, "Measuring the acoustoelectric interaction constant using ultrasound current source density imaging," *Phys. Med. Biol.*, vol. 57, no. 19, 2012, doi: 10.1088/0031-9155/57/19/5929.

[16] Q. Li, R. Olafsson, P. Ingram, Z. Wang, and R.S. Witte, "Measuring the acoustoelectric interaction constant in cardiac tissue using ultrasound current source density imaging," 2010, doi: 10.1109/ULTSYM.2010.5935998.

[17] J. Malmivuo and R. Plonsey, *Bioelectromagnetism*. New York: Oxford University Press, 1995.

[18] C. Huang, A. Alvarez, C. Preston, J. Kang, M. O'Donnell, and R. S. Witte, "Current Density Mapping of the In Vivo Swine Heart using Multichannel Acoustoelectric Cardiac Imaging," pp. 1–4, 2021, doi: 10.1109/ius52206.2021.9593621.

[19] CDC, "Atrial Fibrillation I cdc.gov," Centers for Disease Control and Prevention, 09-Dec-2019. [Online]. Available: https://www.cdc.gov/heartdisease/atrial fibrillation.htm. [Accessed: 06-Jan-2020].

[20] European Heart Rhythm Association et al., "Guidelines for the management of atrial fibrillation: the Task Force for the Management of Atrial Fibrillation of the European Society of

Cardiology (ESC)," Eur. Heart J., vol. 31, no. 19, pp. 2369-2429, Oct. 2010, doi: 10.1093/eurheartj/ehq278.

[21] Lesh, M.D., G.F. Vanhare, D.J. Schamp, W. Chien, M.A. Lee, J.C. Griffin, J.J. Langberg, T.J. Cohen, K.G. Lurie, and M.M. Scheinman, Curative Percutaneous Catheter Ablation Using Radiofrequency Energy for Accessory Pathways in All Locations - Results in 100 Consecutive Patients. Journal of the American College of Cardiology, 1992. 19(6): p. 1303-1309.

[22] Klemm, H.U., O. Franzen, R. Ventura, and S. Willems, Catheter Based Simultaneous Mapping of Cardiac Activation and Motion: A Review. Indian Pacing and Electrophysiology Journal, 2007. 7(3): p. 148-159.

[23] Packer, D.L., Three-Dimensional Mapping in Interventional Electrophysiology: Techniques and Technology. Journal of Cardiovascular Electrophysiology, 2005. 16(10): p. 1110-1116.

[24] Perkins, C. (2022). Multichannel Transcranial Acoustoelectric Brain Imaging in a Human Head Model. *Master of Science-Biomedical Engineering Thesis*.

[25] Preston, C. (2022). Acoustoelectric Imaging of Deep Brain Currents. *Doctor of Philospohy – Biomedical Engineering Dissertation.*

[26] Springer Nature: Springer Nature, “Anatomy and Physiology of the Cardiac Conduction System” by Paul A. Iaizzo, Timothy G. Laske, 2010, under License 5078470511333 (https://link.springer.com/book/10.1007/978-1-4419-6658-2)

[27] “Stimulus Generator Manual STG 4004 and STG 4008.”

[28] Şen, Taner et al. “Mechanical index.” Anatolian journal of cardiology vol. 15,4 (2015): 334-6. doi:10.5152/akd.2015.6061.

Appendix:

List of Publications

1. A. Alvarez, C. Preston, **T. Trujillo**, C. Wilhite, A. Burton, A. Barragan, C. Ingram, R. S. Witte. “Mapping Cardiac Electromechanical Coupling using Acoustoelectric Echocardiography.” *American Physician Scientist Association (APSA) West Regional Meeting*. Loma Linda, CA. November 2019.
2. A. Alvarez, C. Preston, **T. Trujillo**, C. Wilhite, A. Burton, A. Barragan, C. Ingram, R. S. Witte. “Mapping Cardiac Electromechanical Coupling using Acoustoelectric Echocardiography.” *American Medical Association (AMA) EXPO Research Poster Competition*. San Diego, CA. November 2019.
3. A. Alvarez, C. Wilhite, C. Preston, **T. Trujillo**, A. McArthur, D. Mustacich, R.S. Witte. “4D Cardiac Activation Wave Mapping in In Vivo Swine Model using Acoustoelectric Imaging.” *Institute of Electrical and Electronics Engineers (IEEE) International Ultrasonics Symposium*. Glasgow, Scotland. October 2019.
4. **T. Trujillo**, M. Allard, A. Alvarez, C. Preston, R. S. Witte. “Transcranial Acoustoelectric Imaging of Spatially and Temporally Varying Electrical Currents to Better Understand Neuronal Dysfunction.” *Institute of Electrical and Electronics Engineers (IEEE) International Ultrasonics Symposium.* Venice, Italy. October 2022.
5. **T. Trujillo**, M. Allard, A. Alvarez, C. Preston, R. S. Witte. “4D Transcranial Acoustoelectric Brain Imaging of Spatially and Temporally Varying Current Sources in a

Human Head Model." *National Institutes of Health (NIH).* Virtual Attendance. August 2022. (poster).

6. **T. Trujillo**, M. Allard, A. Alvarez, C. Preston, R. S. Witte. "Transcranial Acoustoelectric Imaging of Spatially and Temporally Varying Electrical Currents to Better Understand Neuronal Dysfunction." *Arizona Photonics Days – University of Arizona.* Tucson, AZ, USA. January 2023.